Colloid & Polymer Science Colloid Polym Sci 272:1329–1343 (1994)

Original Contributions

Electron spectroscopic imaging-techniques for the investigation of multiphase polymer systems: Poly(styrene-b-methylphenylsiloxane) thin films*)

A. Du Chesne, G. Lieser, and G. Wegner

Max-Planck-Institut für Polymerforschung, Mainz, FRG

*) *Dedicated to Prof. Dr. E.W. Fischer on the occasion of his 65th birthday with the very best wishes for successful and rewarding research activities in the years to come. The foundations for this work were laid in 1965 when Prof. Fischer introduced his former student G.L. to the elements of electron microscopy, and in 1968, when he convinced G. W. – at that time his assistant – of the importance of electron microscopy as a research tool in structural chemistry*

Abstract: Electron spectroscopic imagining (ESI) is a recently developed method which broadens the scope of electron microscopic imaging considerably. Phase separated diblockcopolymers of poly(styrene) (PS) and poly(methylphenylsiloxane) (PMPS) and their mixtures with the respective homopolymers exhibit domains which differ in elemental composition. One of the phases contains only carbon and hydrogen, the other one contains silicon and oxygen atoms in addition. This feature makes the systems a candidate to demonstrate the application of ESI to problems in polymer material science. Effects of solvent and surface phenomena were studied in unstained thin solution cast films prior to and after annealing. Elemental maps are compared with micrographs which were exposed at an energy loss for which so called structure sensitive contrast predominates. Both methods utilize the inelastically scattered electrons for imaging.

Key words: Electron energy loss spectroscopy (EELS) – elemental mapping – electron spectroscopic imaging (ESI) – morphology of thin films of blockcopolymers of poly(styrene) and poly(methylphenylsiloxane)

Introduction

The determination of shape, size and size distribution of domains in phase separated multicomponent polymer materials is a frequent task in electron microscopy and a basic problem in polymer material science.

Phase separation of the components of a blockcopolymer can only take place on a length scale, typically of the order of 10 nm, related to the radii of gyration of the individual blocks. Phase segregated blockcopolymers form various morphologies (also known as ordered state) in thermodynamic equilibrium as a function of composition according to the principle of minimal surface [1–3]. Investigation of block copolymer morphology is therefore a domain of transmission electron microscopy (TEM) [4–6].

Varying elastic scattering power as a function of the atomic number Z of the elements at distinct sites of the sample leads to contrast which, in addition, depends on specimen thickness and density of the components. Since common polymers consist mainly of hydrogen and carbon and usually do not contain heavy elements, their densities are similar and therefore contrast is, in general, poor. In particular, when the components of a polymer mixture or a block copolymer are amorphous, investigations by electron microscopy are only promising if the contrast can be

enhanced by selective staining of one component. Reactivity of the constitutive units of one block is therefore a prerequisite to discriminate various phases in a sample. Thus, most what is known about the morphology of phase separated block copolymers originates from systems in which one of the blocks contains unsaturated bonds for which staining by osmium tetroxide (OsO_4) is a conventional method of contrast enhancement [4–10].

However, there are many cases where appropriate staining methods have not yet been established. Recent development in TEM design provided access to overcome the problem of lacking contrast in the case where heteroatoms are concentrated in distinct phases of the sample. Instead of contrast enhancement by staining, the effect of inelastic interaction of the electrons with the material is utilized to discriminate phases locally.

Inelastic scattering at the inner shells of atoms causes element specific energy losses of the electrons transversing the sample [11–13]. Electron energy loss (EEL-) spectrometers corrected for imaging errors have been integrated into the projective system of a TEM [14–21] or have been adapted below the final screen [22]. They allow not only to record EEL-spectra but also electron spectroscopic images (ESI) and electron spectroscopic diffraction (ESD). All options of conventional TEM (CTEM) are maintained and, in addition, the effect of chromatic aberration on the final image is eliminated. All experimental techniques and methods which use the integrated spectrometer are generally summarized in the literature as "energy filtering transmission electron microscopy" (EFTEM) [23, 24]. EFTEM is particularly valuable in polymer science because a wide variety of polymer systems offer only low contrast but possess different elemental compositions of their components. It is therefore surprising that only a few results using this method on polymers have been published yet [25–29].

The main body of this paper is centered around investigations on the morphology of thin films of a diblockcopolymer PS-b-PMPS (Scheme 1) consisting of poly(styrene) (PS) and poly(methylphenylsiloxane) (PMPS). This polymer system, for which a staining method is not known, has the peculiarity that its components are partially miscible. Synthesis and characterization by means

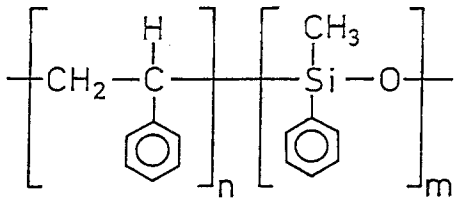

PS–b–PMPS

of other experimental methods have been described elsewhere [30–34].

CTEM failed to provide sufficiently detailed information about the morphology of the samples by ordinary bright field images because the contrast between the components is too small. This was unexpected in so far as another system with poly(dimethylsiloxane) instead of PMPS blocks exhibits sufficient contrast to be imaged in bright-field [35]. This feature can be explained on theoretical grounds, however. The presence of the heteroatoms silicon and oxygen in the PMPS component of the block copolymer makes it a candidate for EFTEM. First results of the investigations on the bulk morphology by EFTEM have been published elsewhere [29, 32]. In this contribution we want to highlight the efficiency of the new technique by presenting investigations on thin solution cast films.

Experimental

Samples

Synthesis and characterization of PS-b-PMPS are described elsewhere [30–32]. Some characteristic parameters of the sample CP1 to CP5 are listed in Table 1. The data originate (under different designation) from these papers.

Sample preparation

Thin films were cast from 0.5 wt.% solutions of the polymers in one of the solvents dichloromethane, tetrahydrofuran (THF), toluene or cyclohexane. Three to four drops of the solution were put on a microscope slide with or without carbon coating. In an attempt to ensure microphase separation, the evaporation rate of the solvent was slowed by placing the slide onto several sheets of

Table 1. Characterization of the investigated A-B diblock copolymers PS-b-PMPS (CP1-CP5) [30–32].

Sample	$\bar{M}_n$ [g.mol^{-1}]	$\bar{M}_w/\bar{M}_n$	W_{PMPS}	Φ_{PMPS}	T_g(PS) [°C]	T_g(PMPS) [°C]	T_{ODT} [°C]
CP1	56500	1.03	0.240	0.225	88	− 27	99
CP2	56000	1.04	0.350	0.331	97	− 25	147
CP3	63800	1.06	0.419	0.399	91	− 27	184
CP4	56400	1.06	0.520	0.499	96	− 25	164
CP5	59000	1.05	0.770	0.754	87	− 26	129

$\bar{M}_n$: number average molecular weight, determined by osmometry
$\bar{M}_w/\bar{M}_n$: polydispersity, determined by GPC
$W_{(PMPS)}$: weight fraction of the siloxane component, determined by ^{1}H–NMR and elemental (Si) analysis
$\Phi_{(PMPS)}$: volume fraction of the siloxane component at room temperature
$T_{g(PS)}$, $T_{g(PMPS)}$: glass transition temperatures of the components as determined by DSC

Table 2. Characterization of the mixture M3

M3:	CP4	block PS	PMPS	homo PS	PMPS	total PS	PMPS
mass fraction n	0.33	0.17	0.16	0.49	0.18	0.65	0.35
vol. fraction Φ	0.325	0.175	0.15	0.505	0.17	0.68	0.32
M_n(osm.)	55400	28800	26600	45000	100000		
P_n	470	274	196	429	735		

filter paper soaked with about 10 drops of solvent inside a Petri dish which was subsequently covered by a lid. Some of the films were annealed in a vacuum oven at various temperatures.

Solution cast thin films of the mixture M3 of CP4 with both homopolymer constituents (for the characterization see Table 2) were prepared from a 0.5 wt.% solution in toluene. All films were floated off onto water and transferred onto hexagonal 600 mesh copper grids.

Electron spectroscopic imaging (ESI) and Electron Energy Loss Spectroscopy (EELS)

TEM observations were performed either with a Zeiss EM 902 (operated at 80 kV) or a Zeiss EM 912Ω instrument (operated at 120 kV).

Micrographs were recorded on Kodak SO-163 sheet film or on Ilford Pan F 35 mm film. The width of the energy window δE used was 20 eV in the case of the EM 902 and 10 eV for the EM 912Ω. Some images in the latter instrument were recorded digitally via a silicon intensified target (Dage SIT-66) camera and processed by a Kontron/Zeiss IBAS image processing system. Processed images were transferred to Ilford Pan F photographic film via a photorecorder Montage FR1 (resolution 512×512 pixels and 256 grey values). Elemental distribution images were performed in the same way.

EEL-spectra were recorded sequentially with the Zeiss EM 912Ω at 120 kV in the spectrum mode. The spectrum was shifted in 0.2 eV- steps over the energy selector slid of width $\delta E \cong 1.0$ eV. Hence the energy resolution is limited by the energy dispersion of the primary electrons, which was determined to be 1.6 eV (half width of the zero-loss peak for a tungsten filament at illumination angle 0.1 mrad at an emission current of 4μA).

Principles of energy filtering

Contrast is the essential prerequisite to the detection of a heterogeneity inside a matrix. In the present case, where we deal with the morphology of a polymer mixture or a blockcopolymer of the components PS and PMPS, the considerations can be restricted to amorphous material ignoring

Bragg contrast which would arise from crystallites. Contrast in TEM images is mainly produced by scattering of electrons inside the sample involving both elastic and inelastic processes. The scattered intensity is a function of the density of the nuclei, their atomic number and the sample thickness. The contribution of elastically scattered electrons to image formation can be controlled by the size of an objective aperture. The angles into which electrons are scattered inelastically in a single event are so small that they cannot be cut by apertures and pass all diaphragms inside a conventional transmission electron microscope (CTEM) deteriorating the quality of an image with increasing sample thickness by the effect of chromatic aberration.

The quantitative measure of the scattering power relates to the scattering cross-sections for elastic and inelastic processes. Contrast between two phases can be expressed by the normalized difference of transmission of electrons through both phases. The transmission is defined as the fraction of electrons which either remain unscattered or are scattered through angles inside an objective aperture α. According to Reimer et al. [24, 36–38] the transmission $T(\alpha)$ can be written as a function of sample thickness t and objective aperture α

$$T(\alpha) = \exp[-t \cdot N_s \cdot \sigma_t(\alpha)] , \quad (1)$$

N_s being the number of scattering centers per volume and σ_t (α) the partial scattering cross-section of the corresponding element for all scattering angles $\Theta \geq \alpha$. Here, the total scattering cross-section represents the sum of elastic and inelastic cross-sections. We take advantage of this additivity in order to evaluate the contrast in the investigated polymer system and use the following equation

$$T(\alpha) = \exp\left[-t \cdot N_s \cdot \sum_i n_i \cdot \sigma_{ti}(\alpha)\right] , \quad (2)$$

where n_i is the mole fraction of element i and $\sigma_{ti}(\alpha)$ the corresponding total cross section. Elastic cross-sections were calculated according to Lenz [39] using the following equations

$$\sigma_{el} = 1.87 \times 10^{-6} \cdot \frac{Z^{4/3}}{\beta^2} \quad (3)$$

and

$$\sigma_{el}(\alpha) = \frac{\sigma_{el}}{1 + (\alpha/\Theta_0)^2} , \quad (4)$$

where β equals v/c, i.e., the ratio of the velocities of the electrons and of light, and Z is the atomic number. $\Theta_0 = \lambda/2\pi R$ is the characteristic elastic scattering angle with the de Broglie wavelength λ and the "atomic radius" $R = a_H \cdot Z^{-1/3}$, a_H being the Bohr radius [24]. According to Reimer et al. [38] the inelastic scattering cross-section σ_{in} can be estimated by $\sigma_{in} = 20 \cdot \sigma_{el}/Z$. The angular dependency of σ_{in} is, however, different from that of σ_{el} and can be formulated [39] as

$$\sigma_{in}(\alpha) = \frac{\sigma_{el}}{Z}\left[\frac{-1}{1 + (\alpha/\Theta_0)^2} + 2\ln(1 + \Theta_0/\alpha^2)\right] \quad (5)$$

Using these equations, one can formulate both global and elastically filtered transmission. Figure 1a displays calculations of the transmission at a high voltage of 120 kV for phases of uniform thickness for the components of the frequently investigated blockcopolymer of polyisoprene (PI) and poly(styrene) (PS). The difference of transmission between both components is very small for CTEM. It increases with decreasing size of the objective aperture at the expense of the absolute value of transmission. Another important result is the strong decrease of transmission when an energy selector is inserted, in which case the contrast vanishes almost completely in the example of PS-PI.

The contrast between the phases of this blockcopolymer is insufficient to discriminate between adjacent domains of different phases in conventional brightfield images obtained by either CTEM or EFTEM. In order to circumvent this problem the actual system is usually stained, i.e. the unsaturated component PI is selectively reacted with OsO_4 thereby increasing the contrast significantly. This is shown in Fig. 1b under the assumption that PI is converted to poly(0.5 OsO_4-isoprene) upon staining. As in Fig. 1a the calculated difference of transmission between both components is smaller in the filtered than in the unfiltered case. Elastically filtered electron micrographs, however, are in practice more sharply defined, because the inelastic fog originating from electrons which are not focussed onto the final screen has disappeared. Figure 1c displays

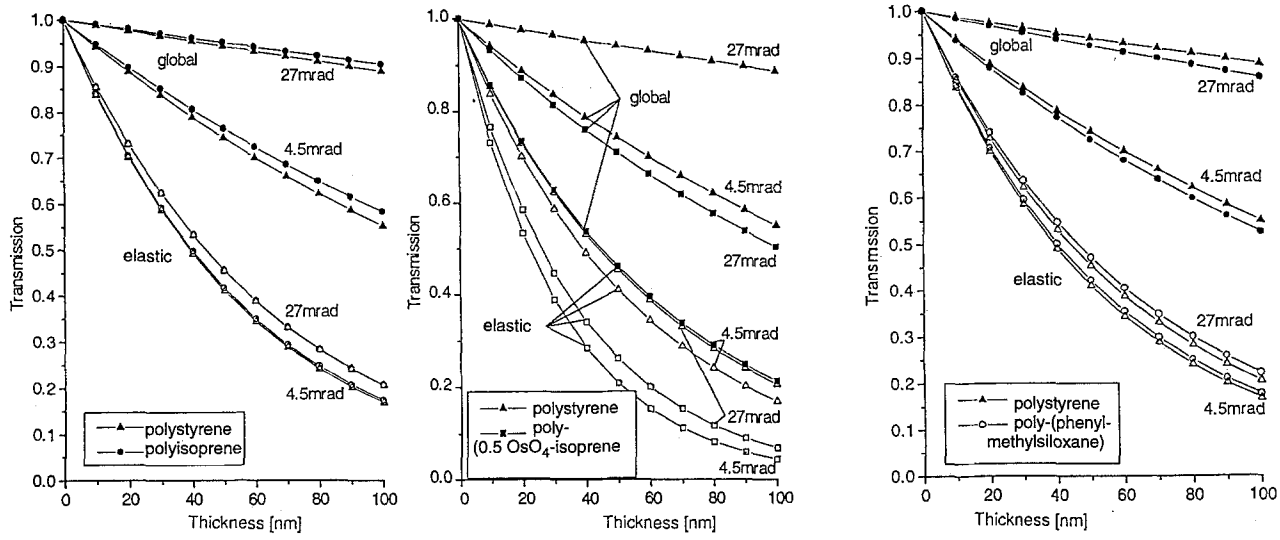

Fig. 1. Transmission for the systems a: PS-PI, b: PS-poly(0.5 OsO_4-isoprene) and c: PS-PMPS; scattering cross-sections are calculated using Lenz's theory [39]. (For b it is assumed that every second repeating unit is stained by one OsO_4 without volume expansion to occur)

the transmission calculated for the system PS-PMPS. Both global and elastic brightfield images do not exhibit sufficient contrast in complete agreement with observation.

The appropriate method to overcome the problem of contrast deficiency in samples of PS-b-PMPS diblock copolymers is EFTEM, which takes advantage of the presence of silicon and oxygen in only one of the components. Inelastic interactions of the electrons of the incoming beam with inner shell electrons of the atoms of which the sample is composed give rise to distinct energy losses the magnitudes of which are characteristic for each element. The position of the absorption edges on an energy scale is displayed in Fig. 2 representing the EEL spectrum of the block copolymer CP3. The silicon K- and $L_{2,3}$-edges are found at 1840 eV and 99 eV, the oxygen K-edge at 532 eV and the carbon K-edge at 283 eV. Si and O K-edges are evident in the spectra as recorded; the Si $L_{2,3}$-edge which is superimposed to the steep slope of the plasmon region is shown with the background subtracted. For this purpose the background under the absorption edge is extrapolated from a region of energy loss below the absorption edge but adjacent to it by a least square method. In order to determine the local distribution of a particular element in an image the same procedure has to be performed pixelwise

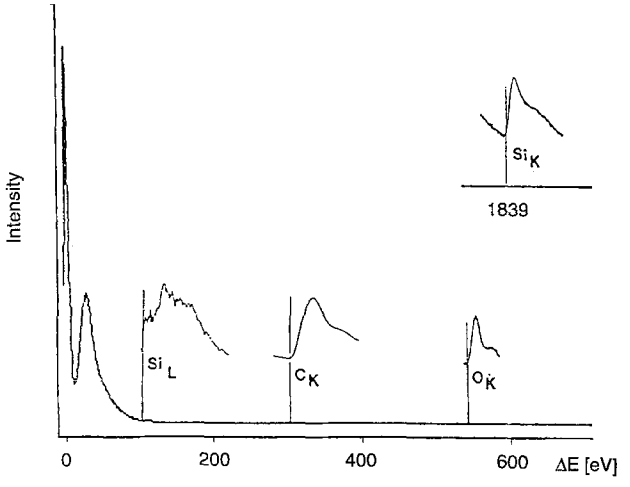

Fig. 2. EEL-spectrum of CP3 exhibiting Si L-, C K-, O K- and Si K-absorption edges. Intensities in areas of absorption edges are amplified, mass thickness background was stripped in case of the Si-L-absorption edge (120 kV, objective aperture $\alpha = 27$ mrad, width of energy selecting slit $\delta E \cong 1$ eV)

in the imaging mode. However, due to the limited capacity of the memory it is impossible to use a large number of points for extrapolation. Provided that the background intensity can be described by a power law 2 experimental points taken at energies below the absorption edge are

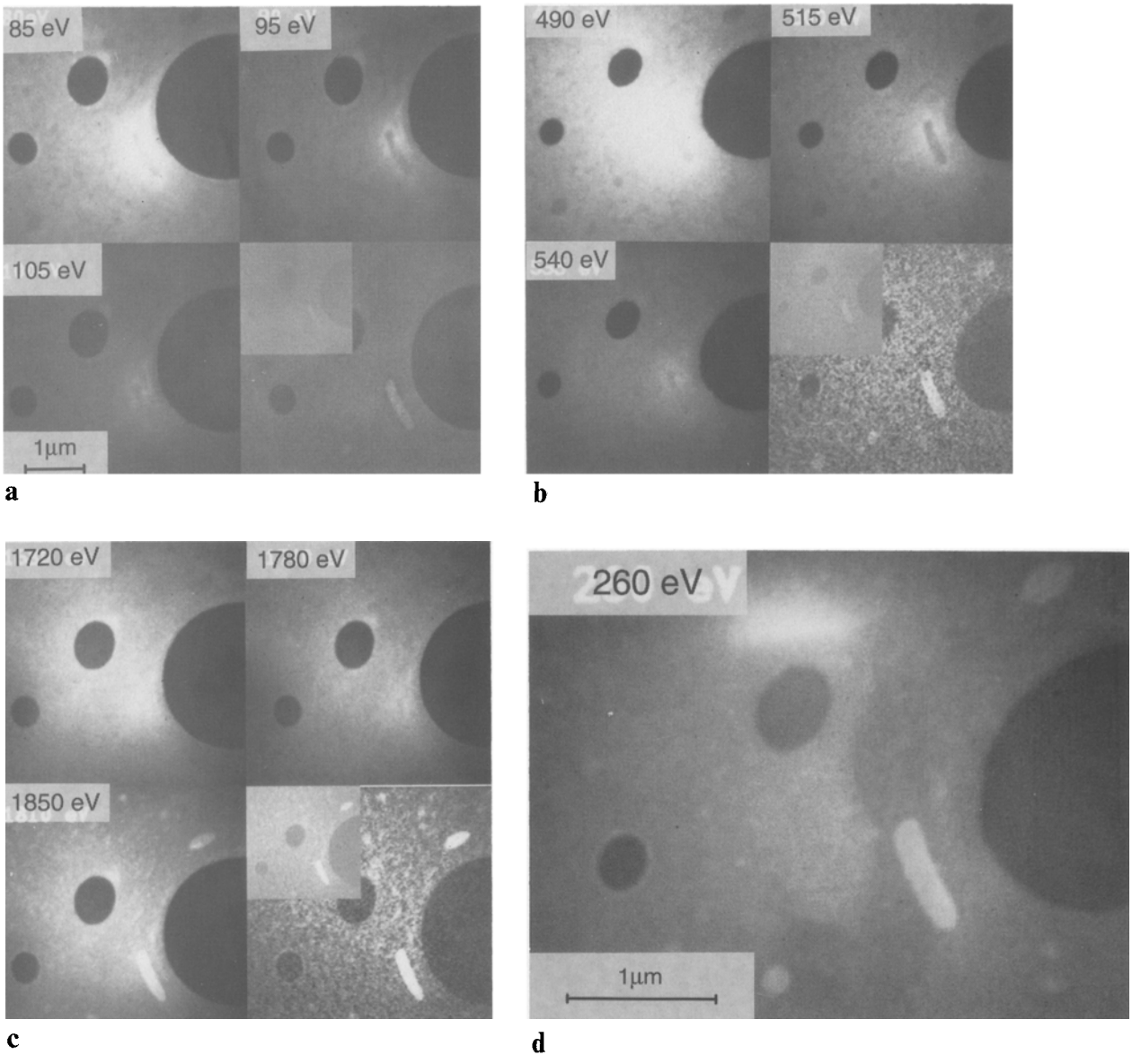

Fig. 3. Silicon and oxygen mapping of a thin solution cast film of the blend M3. a: Si-$L_{2,3}$- edge, b: O-K- edge, c: Si-K-edge. The partial images on top and bottom left represent the original 3 ESI images used to obtain the elemental distribution, and the partial images at bottom right are elemental maps. The inserts at lower magnification within the elemental maps are the original difference images shown without contrast enhancing. d: digitized ESI-image at $\Delta E = 260$ eV without contrast enhancing. The micrograph displays SSC between PMPS- and PS- phases. Siloxane domains appear as the brighter ones. (120 kV, $\alpha = 4.5$ mrad, $\delta E = 10$ eV)

sufficient to find the base line in a double logarithmic plot. One finds this assumption experimentally justified in many cases and hence, this simplified procedure was used in all cases discussed here to calculate elemental maps.

Figure 3 shows the raw images (denoted by the respective energy losses ΔE) and elemental maps for a solution cast film of the mixture M3 (c.f. Table 2). In this case phase separation between a mixture of the block copolymer with homo PS (matrix) on one hand and homo-PMPS at the other hand takes place at a large scale. The selected area contains large domains of the PMPS phase, the matrix and a hole. Figure 4 represents a

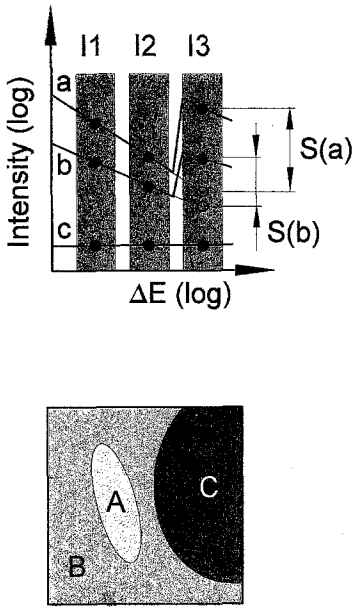

Fig. 4. Sketch of the procedure of elemental mapping of a specimen modeling the sample shown in Fig. 3. Area A: pure PMPS macrophase, B: matrix consisting of PS and PS/PS-b-PMPS, C: hole. a, b. and c assign schematic EEL-spectra (on a double logarithmic scale) which correspond to the areas A, B, C. I1-I3 represent the position ΔE of the energy windows used to record the three images necessary for elemental mapping. Filled circles: experimental values, open circles: extrapolation. S(a) and S(b): net element specific signal

sketch of these three regions and of the corresponding EEL spectra. Region A (EEL spectrum a) represents the PMPS phase, B (b) the matrix and C (c) the hole. The raw images are taken at the positions I1 and I2 below and at the position I3 above the absorption edge. The filled circles represent measured intensities, the open circles extrapolated values. The straight lines a and b show different slopes. The absorption edges have different step heights, representing different concentrations of PMPS in regions A and B, c is horizontal, because the intensity within the hole remains zero. According to the differences between the measured and the extrapolated values at position I3 region A is shown as very bright on the elemental map, B appears as gray, and the area of the hole is black. This behavior can be verified in the experiment independent from the edge used (Fig. 3, bottom right of each series). The inserts at half magnification are the elemental maps obtained directly after the subtraction, the main pictures show the elemental maps after contrast enhancement. The granularity seen in the image reflects electronic noise mainly from the intensifying camera which, of course, is also amplified via contrast enhancement and should not be interpreted as an effect of varying elemental concentration.

Recalling that the actual problem was to produce images of the morphology of microphase separated diblock copolymer samples, we were not able to produce elemental maps on the grounds of technical problems: morphological subunits of a demixed block copolymer have dimensions in the order of magnitude of 10 nm. Magnifications of $5 \cdot 10^4$ times and larger are necessary to discriminate the subunits. The intensities in the region of either the K-edges of silicon or oxygen turned out to be too low in this range of magnification to register three images with a sufficiently low noise level; intensities of the Si L-edges which are superimposed to the slope of the plasmon region could not be used either because the dynamical range of the SIT camera was not sufficient.

However, for the purpose of discriminating adjacent domains of the block copolymer in an image, one can take advantage of another property of the EEL spectra of the components. Beyond an energy loss of about 50 eV the probability of an inelastic event decreases continuously and comes to a minimum just below the carbon absorption edge. Inside PMPS domains the continuous slope originates from scattering at the carbon atoms to which intensity from the silicon L-edges is superimposed. Its relative contribution to the total intensity is therefore at its maximum when the contribution of carbon is at its minimum. One can expect that a PMPS domain differs from an adjacent PS domain by contrast the former appearing brighter in the image, at least when both are of equal thickness. This effect leading to enhancement of the contrast by inner-shell losses of heteroatoms concentrated in domains is denoted as "structure sensitive contrast" (SSC). The expression might be misleading for polymers, but it has meanwhile been introduced into the literature [24, 38]. Images which show heterogeneities by SSC can be recorded on photographic film in the conventional manner taking advantage of the much higher resolution offered by a photographic film as compared to a digitized image on a monitor. In comparison to elemental

mapping the possibility to analyze composition quantitatively is lost in SSC because effects of varying mass thickness cannot be sharply separated from effects of composition. However, in absence of very strong fluctuations of thickness the element specific information appeared to be the dominating feature in images of samples containing domains of PS and poly(siloxanes) [40]. A more quantitative consideration of SSC in the case of PS-b-PMPS is given in the appendix. Figure 3d depicts the same region of the sample M3 in SSC at an energy loss of 260 eV. The micrographs of Fig. 3 verify that images in SSC give the same information as the ones obtained by element specific contrast. The siloxane domains appear as the brighter ones.

Application of EFTEM to the investigation of thin solution cast films of PS-b-PMPS diblock copolymers

Thin films of block copolymers are frequently prepared by solution casting. This gives rise to solvent effects in the morphology. If the solvent is a selective one for block A, block B will start to form micellae at a critical concentration in the course of solvent evaporation, while block A remains solvated. The nonuniform distribution of solvent between the components leads to a change of the volume fractions of the segregating phases with respect to the pure components at the order-disorder-transition (ODT). The type of the developing morphology may thus be altered. Such solvent effects can only be removed by heating the polymer films above the ODT temperature [41].

Surface effects may strongly influence the morphology of thin block copolymer films as well. This was shown for thin film droplets of poly(styrene butadiene) blockcopolymers by Henkee et al. [42] by means of CTEM using stained samples. A spinodal wave may be induced by a surface even far above the microphase separation temperature [43, 44].

The effect of SSC is demonstrated by Fig 5 with a thin film of the diblock copolymer sample CP5 which contains PS as the minor phase. The film was cast from dichloromethane solution onto a carbon coated glass slide. The series of 4 micrographs in Fig. 5 displays the contrast as a function of the energy loss ΔE. In agreement with the results shown in Fig. 1c the elastic brightfield image (Fig. 5a) does not show any contrast at all with the exception of a circular dark area (bottom left) where the sample exhibits higher thickness. At an electron energy loss of 80 eV (Fig. 5b) the contrast of this thicker area is inverted. In addition, a weak modulation of gray values can be seen that reflects mass thickness fluctuations. This modulation is significantly enhanced at 120 eV (above the Si $L_{2,3}$-edge) (Fig. 5c). The contrast then increases continuously toward the carbon K-edge as is demonstrated by the image taken at an energy loss of 270 eV in Fig. 5d. At this energy loss the contribution of electrons having interacted with carbon atoms only is at minimum. The different components can now be discriminated as distinctly in the SSC mode as can be similar structures of an OsO_4 stained PS-b-PI block copolymer imaged in conventional brightfield.

Solution cast films which were not annealed after preparation always exhibited a more or less granular structure independent of the composition of the polymer, the kind of solvent (dichloromethane, THF, toluene and cyclohexane) and its evaporation rate. Figure 6 displays an electron micrograph of the sample CP4 cast from toluene as an example. This sample is expected to have lamellar structure in the bulk but only an unspecific granulation is observed. It is worth mentioning that PS-b-PMPS does not differ from PS-b-poly(butadiene) solution cast films imaged after staining with OsO_4 [45].

As already mentioned, the morphology of block copolymers prepared from solution is determined by the formation of micellae when a critical concentration is exceeded [41, 46, 47]. With increasing micelle concentration a regular morphology is developed and maintained in the bulk after all solvent is removed. Thus the solvating properties of a particular solvent account for variations in the morphology at a distinct composition. However, our observations on thin films did not clearly reveal how the kind of solvent modifies the morphology. One reason might be that solvent evaporation during film preparation was not slow enough to establish equilibrium conditions. In addition, solvent effects cannot be separated from the influence of the solid surface of the substrate. It is usually the component with the lowest surface free energy which is in contact with the substrate thereby developing a basal layer. This

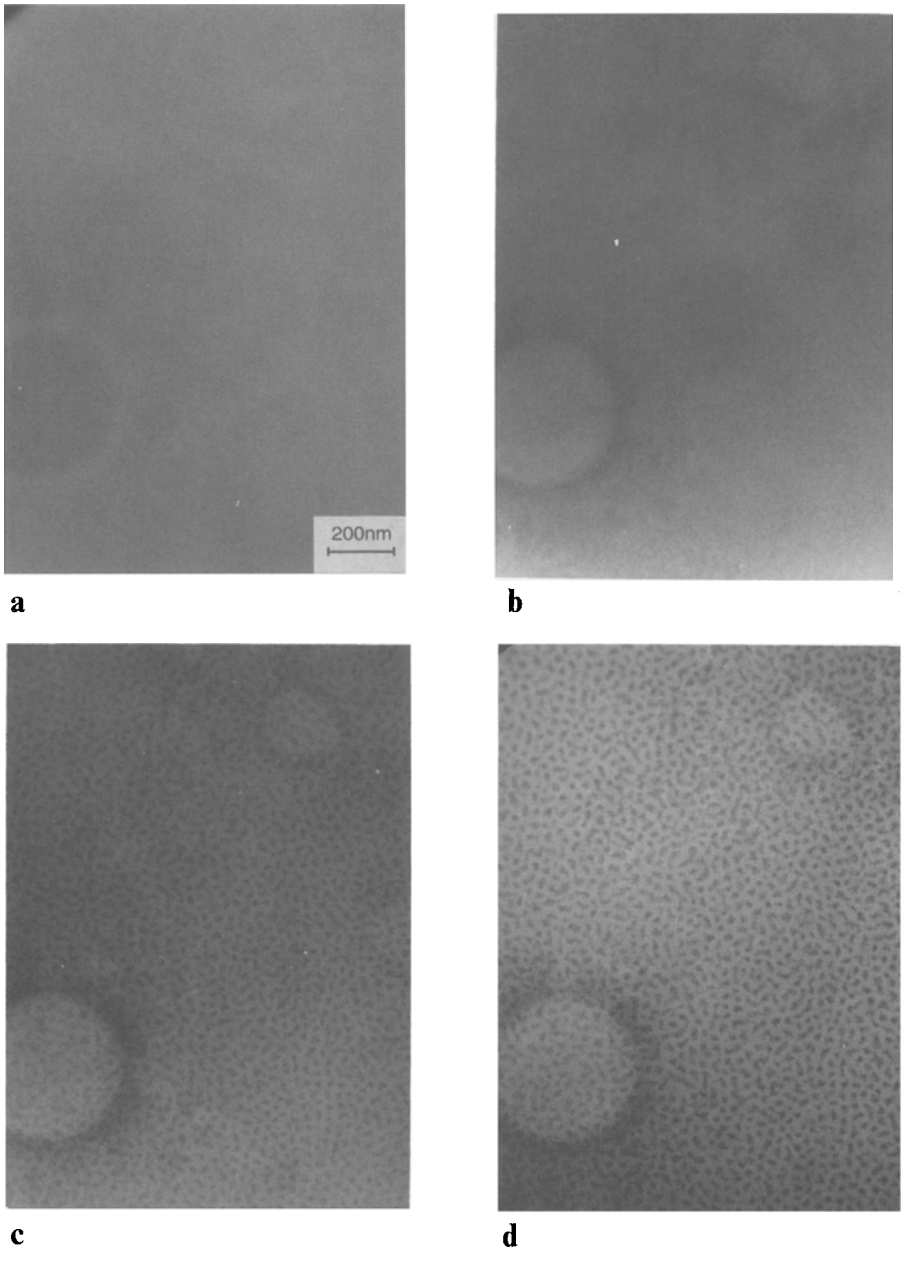

Fig. 5. ESI-images of a solution cast thin film of CP5 on a carbon substrate. a: $\Delta E = 0$ eV (elastic brightfield), b: $\Delta E = 80$ eV, c: $\Delta E = 120$ eV, d: $\Delta E = 270$ eV (80 kV, $\delta E = 20$ eV, $\alpha = 8$ mrad)

leads simultaneously to an excess volume of both, the surface active compound at the surface and of the other compound in the adjacent volume. The morphology is therefore expected to vary as a function of the distance from the solid surface. In a thin film, transparent enough for TEM observation, the width between the outermost surfaces is not sufficiently large to reach the state in which the composition has its average bulk value.

In order to avoid such effects the films were annealed at temperatures above the order-disorder transition. During annealing the films disintegrated into islands of nonuniform thickness which are not everywhere transparent enough for the electron beam. But this feature allowed the investigation of films of various thicknesses prepared under totally identical conditions. As expected, morphologies of one of the types formed

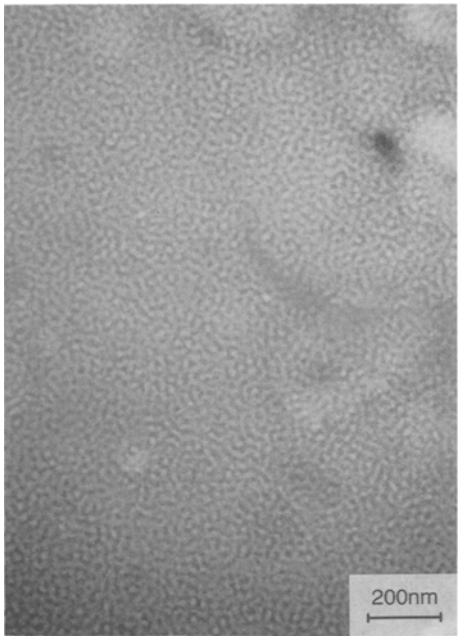

Fig. 6. ESI-image of a thin film of CP4 cast from toluene solution on a carbon substrate (80 kV, $\Delta E = 260$ eV, $\delta E = 20$ eV, $\alpha = 8$ mrad)

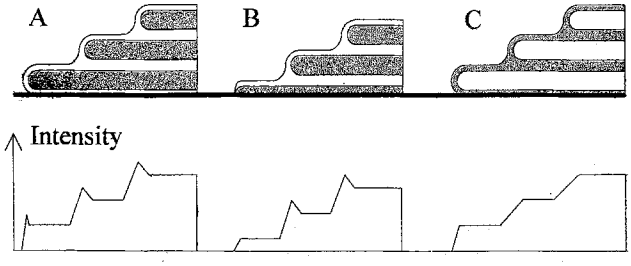

Fig. 7. Sketch of various stacking of layers in outermost areas of thin films of PS-b-PMPS (top) and the respective brightness profiles which are expected in ESI micrographs (SSC)

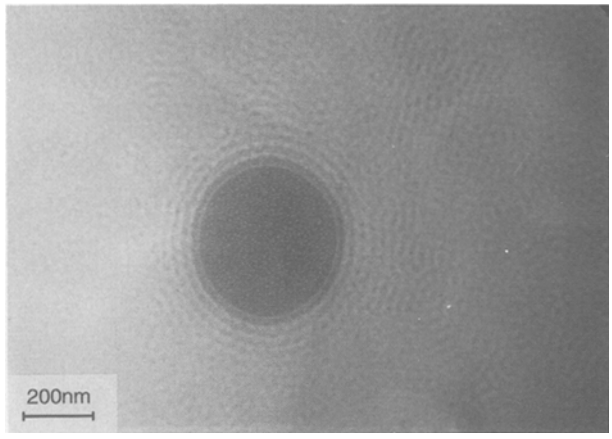

a

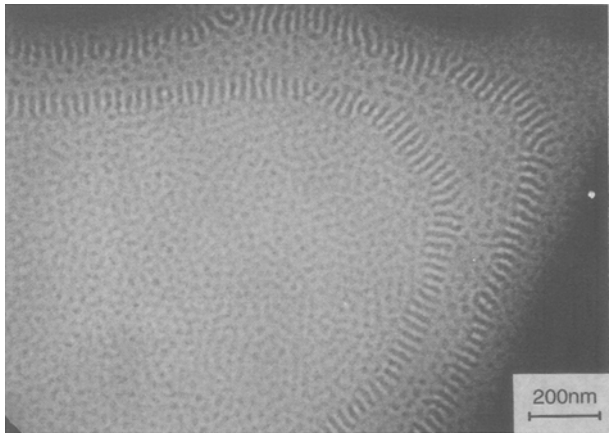

b

Fig. 8. ESI-micrographs of thin films of CP3 on a carbon substrate. a: cast from cyclohexane solution and annealed at 195 °C, b: cast from methylenedichloride solution and annealed at 145 °C (80 kV, $\Delta E = 260$veV, $\delta E = 20$ eV, $\alpha = 8$ mrad)

under thermodynamic equilibrium conditions in bulk [3, 4, 6] are not seen in the annealed films owing to the predominance of interactions with both the solid surface of the substrate and the free surface.

The tendency that only one component likes to make contact with the substrate favors a stepwise increase of the film thickness from the outermost edge of an island to the interior until the modulation of composition is no longer observable. This superstructure is sketched in Fig. 7, neglecting details of the morphology inside a layer (top). The corresponding brightness profiles are shown below as expected from micrographs obtained in SSC mode. A homogeneous layer parallel to the substrate cannot be recognized as such in an ESI micrograph; its existence is deduced from the average gray level of the matrix and the visible composition of the subsequent layer. Figure 8a is an example for case A depicted in Fig. 7. Starting from the central hole, a very tiny white stripe is seen representing the projection of the outermost and basal layer of PMPS. The stripe borders upon a gray area in which two outer layers of PMPS

and one inner layer of PS are superimposed. A similar pattern occurs repeatedly because with increasing film thickness a mesh-like structure of the inner PMPS phase becomes visible. The sample was prepared from a cyclohexane solution of the polymer CP3; it was then annealed at 195 °C (above the order-disorder transition). At this annealing temperature the memory of the film as to which solvent it was cast from is expected to be deleted. The bulk morphology of this polymer is the ordered bicontinuous double diamond structure (OBDD) which is intermediate between lamellar and cylindrical order [6, 48, 49]. Figure 8b illustrates the case C of Fig. 7. The block copolymer was again CP3, but the film was cast from dichloromethane and annealed for 12 h at 140 °C (between the glass transition of PS and the order-disorder transition temperature). Here, one infers from the lack of the outermost white stripe, by the overall higher brightness of the outermost area and by the fact that in this area PS appears as the disperse phase in the second layer that the bottom layer consists essentially of PS. We suggest in this case that primarily a continuous film of PS is formed on the substrate because PS remains dissolved for a longer duration of time than PMPS. At the annealing temperature the mobility of the PS blocks is high enough for the disintegration of the continuous film into islands but not sufficient to allow the disperse PMPS phase to come into contact with the solid surface. The outermost area borders upon a striated rim in which the sample could be lamellar owing to the PMPS excess volume. Proceeding further towards the center the structure changes occasionally exhibiting a hexagonal pattern of cylinders. The pattern is repeated towards the thicker interior of the island. Inside the rims differentiation between lamellae seen edge-on and cylinders parallel to the substrate seems rather meaningless in a film the thickness of which does not significantly exceed the repeat distance between the moieties. Thus far, an unambiguous discrimination is impossible for an electron micrograph. Recalling that the sample CP3 exhibits OBDD morphology in thermal equilibrium, we suggest that we observe lamellae at the rims and cylinders oriented perpendicular to the substrate in between as expression of a quasiperiodic fluctuation round the equilibrium volume composition. Owing to surface effects excess volumina occur repeatedly in both of the components. The amplitude of the fluctuation decreases towards the center of the island. In addition, there is no argument in favor of a sudden change of the orientation of cylinders at the boundary of the rim.

Thin films annealed on a solid substrate have two kinds of surfaces: the one is in contact with the substrate and the other one is free. The interpretation of the electron micrographs may be more complex than suggested because we do not really know whether there are significant differences between the surfaces which we see only in projection. Experiments with free standing films which were performed to eliminate this ambiguity were successful in only one case. Films of the samples CP1 to CP4 were annealed directly on 600 mesh hexagonal electron microscopic grids without any substrate a few degrees below the ODT. With the exception of sample CP2 the films showed to be not self-supporting during annealing. The material of the film wets the mesh bars of the grid which causes thinning of the free standing part followed mostly by rupture. Figure 9 displays the thinned film of CP2. Although PS is the major component in the block copolymer the visible composition is here inverted and PS appears as the disperse phase. The morphology consists of two continuous PS layers with an intermediate layer which exhibits a hexagonal pattern of PS domains. Increasing thickness of the film towards the mesh bar (lower right corner) enables formation of lamellae or cylinders

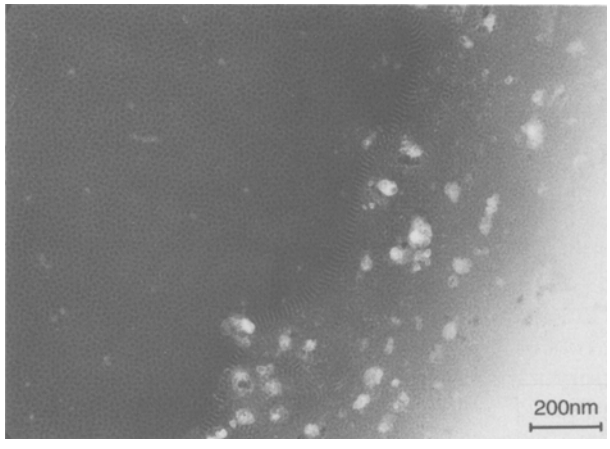

Fig. 9. ESI-micrograph of a free standing thin film of microphase separated CP2 annealed for 12 h at 140 °C. (80 kV, ΔE = 260 eV, δE = 20 eV, α = 8 mrad)

oriented parallel to the direction of flow during annealing. The very bright spots near the mesh bar are assigned to high mass thickness contrast of short range thickness variations and are of no interest here.

Increasing of the annealing time or temperature is followed by further thinning of the film. When a critical film thickness of the order of magnitude of the radii of gyration is reached the structure of the film becomes homogeneous. Such a behavior which was postulated for both thin films of block copolymers and polymer blends [42], was until now only demonstrated for blends [50].

Practical aspects of ESI in comparison to conventional techniques of electron microscopic imaging

Electron spectroscopic imaging is undoubtedly efficient for systems which cannot be stained selectively but which contain heteroatoms in one of their phases. An important parameter for image formation is the local concentration of heteroatoms in the domains to be imaged. It is normally low owing to the dominance of carbon atoms in an ordinary polymer; in the example of PMPS the concentration amounts to only 11 atomic % (ignoring hydrogen atoms). But such a consideration is only valid if the phase extends over the whole sample thickness. Otherwise, additional carbon atoms along the beam path through the matrix have to be taken into account diminishing the effective concentration and therefore the visibility of a domain or parts of it in an electron micrograph. This effect was used in order to evaluate the thickness of the interphase in the investigated system by means of electron microscopy [32].

The main problem for samples with rough surfaces (as are many ultrathin sections in particular) is to differentiate between contributions to the intensity from the presence of heteroatoms and those of varying mass thickness. The appropriate procedure of discrimination between both contributions is elemental mapping. We found the applicability of elemental mapping restricted with our camera equipment to coarse structures of a size of roughly 100 nm. For more detailed structures which need high resolution or for elements with absorption edges at high energy losses the intensities are often not high enough to obtain images sufficiently free of camera noise. For noisy micrograph extrapolation, subtraction of images and subsequent image processing run the risk of producing ghost structures which should not be interpreted in terms of elemental concentration differences. For PS-b-PMPS block copolymers the application of SSC using the excess intensity behind the silicon L-edge adjacent to the C-K-absorption edge was a means to overcome the problem after it was clear from the macrophase separated mixtures that bright areas in the images could be assigned to the siloxane component.

In spite of the restrictions mentioned, the system PS-PMPS is an example for problems the solution of which is obviously significantly facilitated by the method of electron spectroscopic imaging (ESI). For a system which can be treated in both ways, either conventionally by staining or by the new imaging techniques the aspect of practicability or effort in the course of sample preparation becomes predominant in the comparison of the methods. The preparation of bulk samples of PS-b-PMPS for instance needs cryosectioning in comparison to stained PS-b-PI which can be sectioned at room temperature. Staining of the unsaturated PI by OsO_4 is an unpretentious procedure which hardens the sample simultaneously. On the other hand, OsO_4 is very toxic and has to be handled with great care. The number of selective staining reactions is small because they have to satisfy several conditions: they have to proceed in the solid state such that a change in the morphology does not occur; this request is by no means trivial since staining leads to reaction products which change the overall composition and number of components of the system. These features change the system (e.g., homopolymers are transformed into copolymers). For CTEM or for elastic brightfield images it is necessary to introduce heavy elements in such a way that they remain fixed in the sample if it is exposed to the vacuum inside the electron microscope. With the possibility of ESI, one could now consider additional (gaseous) reactions in the solid state, which introduce selectively distinct elements (not necessarily elements of high atomic number) into a polymer. Another aspect is the question of whether polymer samples tolerate the electron doses which are much higher for work with inelastically than for elastically scattered

electrons. This is demonstrated by the overall intensity at 260 eV, which amounts to about 1/1000 of the intensity for the corresponding elastic brightfield (if the specimens are not thicker than 50 nm) giving rise to long exposure times (45–60 s). The PS-b-PMPS block copolymers turned out to be rather insensitive against irradiation damage. There are examples known (e.g., PMMA) where elements cannot be used for ESI techniques because of inherent beam damage followed by evaporation of fragments.

Appendix

The structure sensitive contrast in the system PS-PMPS – a short consideration

In the investigated system strong structure sensitive contrast (SSC) occurs at an energy loss ΔE of the imaging electrons between ca. 200 eV and 260 eV, i.e., below the *C-K* edge where a significant difference is observed between the intensities of electrons having passed PS or PMPS. To characterize SSC one has therefore to take into account the particular excitations which can contribute to energy losses up to 260 eV.

In order to determine the fraction of electrons having lost $\Delta E \leq 260$ eV, we consider the total probability for inelastic scattering and subtract the probability for inelastic interactions leading to $\Delta E > 260$ eV. Thereby we will not take into account Compton-scattering, which at $\Delta E = 260$ eV should be cut off even by very large objective apertures.

As above, scattering cross-sections are used to calculate scattering probabilities. The inelastic cross-section $\sigma_{\Delta E<260}$ for electrons with $\Delta E <$ 260 eV is calculated according

$$\sigma_{\Delta E<260}(\alpha) = \sigma_{\text{in}}(\alpha) - \sigma_{\Delta E>260} \tag{6}$$

using Lenz's theory [39] for each element in the sample; summation yields $\sigma_{\text{in}}(\alpha)$ per repeating unit of PS or PMPS.

Excitations of outer-shell electrons account for plasmon losses and interband transitions leading to low energy losses. Element-specific ionization losses have their origin in inner-shell excitations. In the particular case of PS-b-PMPS only the Si

Table 3. Total and partial inelastic scattering cross-sections in units of 10^{-22}m^2 for elements and repeating units in the system PS-PMPS calculated using Lenz's theory [39] and according to Reimer [24, 36] for instrumental parameters used in the investigation. σ in units of 10^{-22}m^2

Element/ Component	$\sigma_{\Delta E>0}$ for $0 < \Theta < \alpha$			
	80 kV		120 kV	
	$\alpha = \pi$	$\alpha = 8$ mrad	$\alpha = \pi$	$\alpha = 4.5$ mrad
σ(per atom)				
H	1.48	1.35	1.09	0.94
C	2.69	2.22	1.97	1.50
O	2.96	2.39	2.17	1.61
Si	3.57	2.76	2.62	1.85
σ(per repreating unit)				
PS	33.39	28.53	24.49	19.51
PMPS	37.24	31.47	27.31	21.48
σ(inner-shell losses for $\Delta E > 280$ eV)				
PS	0.126	0.126	0.085	0.085
PMPS	0.120	0.120	0.081	0.081
σ(inner-shell losses for $0 < \Delta E < 280$ eV)				
PS	1.435	1.435	0.967	0.967
PMPS	1.740	1.740	1.179	1.179
σ(plasmon losses)				
PS	16.42	16.42	11.48	11.28
PMPS	18.94	18.94	13.28	13.28

$L_{2,3}$- and Si L_1-edges at 99 and 150 eV respectively originate from inner-shell losses and are in the position to transmit information about how silicon is distributed over the sample. No selective oxygen inner-shell signal can contribute to the image intensity in the energy region under discussion because the oxygen K-edge is beyond the carbon K-edge.

Scattering cross-sections for inner shell excitations were evaluated according to Bethe [51], plasmon cross-sections using an approximation given by Reimer [36]. Angular dependence of inner shell scattering cross-sections was ignored, because in our case α is much greater than the characteristic inelastic scattering angle. For the evaluations, we used the actual instrumental parameters under which images were recorded. Results are given in Tables 3 and 4.

It turned out that plasmon excitations are essential beside the Si $L_{2,3}$-, Si L_1-and O L_1-excitation which come into play only for domains of the PMPS component. However, among the cross sections so far calculated for single scattering events are none which yield energy losses in the proximity of 260 eV. Therefore multiple scattering along the beam path through the specimen accounts for energy losses which are selected by the energy window at about 260 eV.

Scattering cross sections per volume S correspond to the absolute scattering probability and were evaluated taking into account density and molecular weight of the repeating units of PS and PMPS. They are listed in Table 5 together with mean free path lengths. From the comparison of mean free path lengths and realistic sample thicknesses (exceeding 50 nm only exceptionally), it follows that for the PS component only plasmon losses are in the position to contribute significantly to the intensity at a ΔE of about 260 eV by multiple scattering. In the PMPS component multiple plasmon scattering is superimposed by the feature of inelastic scattering at the Si L-edges. Prerequisite for the contrasts in which silicon containing domains are visible originates from the fact that the ratio between the intensity offset and the intensity of the background are highest just below the carbon K-edge. It is also worth noting that the contribution of plasmon losses to SSC is quite similar for both components.

Table 4. Ionization cross-sections in units of $10^{-22}m^2$ according to Bethe [51] for elements calculated per repeating unit of component (ionizations of shells in bold letters do not contribute to SSC at 280 eV)

Component	Element-Shell	(ΔE[eV])	σ(80 kV)	σ(120 kV)
PS	H-K	(13.6)	1.435	0.9667
	C-K	(283)	0.1256	0.08463
PMPS	H-K	(13.6)	1.435	0.9667
	O-L_1	(25.7)	0.1661	0.1190
	Si-$L_{2,3}$	(99)	0.1134	0.07641
	Si-L_1	(150)	0.02495	0.01681
	C-K	(283)	0.1099	0.07406
	O-K	(532)	0.00803	0.00541
	Si-K	(1840)	0.00203	0.00137

Acknowledgements

The authors are indebeted to Dr B. Gerharz for supplying the PS-b-PMPS block copolymers, for their characterization, and valuable information. Support by the German Ministry of Research and Technology (BMFT) is gratefully acknowledged.

Table 5. Scattering cross-sections S per volume of the components for inelastic interactions in the region $0 < \Delta E < 280$ eV (in units of $10^5\,m^{-1}$) and mean free path λ (in μm) for the instrument settings 80 kV, $\alpha = 8$ mrad and 120 kV, $\alpha = 4.5$ mrad

Component interaction		PMPS				PS			
		80 kV		120 kV		80 kV		120 kV	
		S	λ	S	λ	S	λ	S	λ
H-K	(13.6 eV)	7.263	1.377	4.893	2.044	8.725	1.146	5.878	1.701
O-L_1	(25.7 eV)	0.841	11.89	0.602	16.60	–	–	–	–
Si-$L_{2,3}$	(99 eV)	0.574	17.42	0.387	25.86	–	–	–	–
Si-L_1	(150 eV)	0.126	79.18	0.085	117.5	–	–	–	–
Plasmon*)	(22.5 eV)	147.9	0.067	103.8	0.096	154.1	0.065	105.9	0.094

*) Values for total and partial plasmon cross-sections (Table 3) corrected by the ratio of calculated and experimentally verified cross-sections for amorphous carbon [24]

References

1. Helfand E. Wassermann ZR (1982) In: Developments in Block copolymers I, Goodman I (ed), Appl Sci Publ, London, new York pp. 99–125
2. Hashimoto T, Shibayama M, Fujimura M, Kawai H, (1983) In: Meier DJ (ed) Block copolymers, Science and Technology, Harwood Academic Publ, Chur, London, New York, pp. 63–108
3. Bates FS, Fredrickson GH (1990) Ann Rev Phys Chem 41:525–557
4. Folkes MJ, Keller A (1973) In: Harward RN (ed) The Physics of Glassy Polymers, Appl Sci Publ, London, pp. 548–598
5. Sawyer LC, Grubb DT (1987) Polymer Microscopy. Chapman and Hall, London, New York
6. Woodward AE (1989) Atlas of Polymer Morphology, Hanser, Munich, Vienna, New York
7. Andrews EH (1963) Proc Royal Soc A277:562
8. Kato K (1966) J Polym Sci, Polymer Letters 4:35–38
9. Hendus H, Illers K, Ropte E (1967) Kolloid Z, Z Polymere 216–7:110–119
10. Aggarwal SL (1976) Polymer 17:938–956
11. Colliex C (1984) In: Advances in Optical and Electron Microscopy Vol 9, Barer R, Cosslet VE (eds) Academic Press, London, New York, pp. 65–177
12. Egerton RF (1986) Electron Energy Loss Spectroscopy in the Electron Microscope, Plenum Press, New York, London
13. Fink J (1989) In: Adv. in Electron. and Electron Physics Vol 75 Hawkes PW (ed), Academic Press, Inc., Boston, San Diego, New York, London, Sydney, Tokyo, Toronto pp 121–232
14. Castaing R, Henry L (1962) Compt Rend Acad Sci (Paris) 255:76–78
15. Henkelmann RM, Ottensmeyer FP (1974) J Micr 102:79–94
16. Egle W, Rilk A, Ottensmeyer FP (1984) In: Electron Microscopy Vol. 1, Csanady A et al (eds), Motesz, Budapest pp 63–64
17. Rose H (1978) Optic 51:15–38
18. Lanio S (1986) Optic 73:99–107
19. Krahl D, Paetzold H, Swoboda M (1990) Proc XIIth Int Congr for Electron Microscopy Vol 2 p 60
20. Bihr J, Benner G, Krahl D, Rilk A, Weimer E (1991) Proc 49th Ann Meeting Electr Micr Soc of America, Bailey GW (ed) San Francisco Press pp 354–355
21. Probst W, Benner G, Bihr J, Weimer E (1993) Adv Mater 5:297–300
22. Gubbens AJ, Krivanek OL (1993) Ultramicroscopy 21:146–159
23. Reimer L, Fromm I, Hirsch P, Plate U, Rennekamp R (1992) Ultramicroscopy 46:335–347
24. Reimer L (1991) Energy Filtering Transmission Electron Microscopy In: Adv in Electron and Electron Physics Vol 81 Hawkes PW (ed) Academic Press, Inc., Boston, San Diego, New York, London, Sydney, Tokyo, Toronto pp 43–126
25. Kunz M, Möller M, Heinrich UR, Cantow H-J (1989) Makromol Chem, Makromol Symp 23:57–72
26. Cantow H-J, Kunz M, Klotz S, Möller M (1989) Makromol Chem, Makromol Symp 26:191–196
27. Freitas Siqueira D, Galembeck F, Nunez S (1991) Polymer 32:990–998
28. Huong DM, Drechsler M, Möller M, Cantow H-J (1992) J Microscopy 166:317–328
29. Du Chesne A, Lieser G, Wegner G (1992) Electron Microscopy, Vol 1 EUREM 92 Granada, Spain, pp 255–256
30. Gerharz B (1991) PhD-Thesis, University of Mainz
31. Gerharz B, Wagner T, Ballauff M, Fischer EW (1992) Polymer 33:3531–3535
32. Gerharz B, Du Chesne A, Cai WZ, Lieser G, Fischer EW (1994) J Materials Sci (submitted)
33. Cai WZ, Schmidt-Rohr K, Egger N, Gerharz B, Spiess HW (1993) Polymer 34:267–276
34. Vogt S, Jian T, Anastasiadis SH, Fytas G, Fischer EW (1993) Macromolecules 26:3357–3362
35. Saam JC, Gordon DJ, Lindsey S (1970) Macromolecules 3:1–4
36. Reimer L (1989) In: Springer Series in Optical Sciences 36, Hawkes PW (ed), Springer, Berlin, Heidelberg, Chapt. 5
37. Reimer L, Ross-Messemer M (1989) J Micr 155:169–182
38. Reimer L, Ross-Messemer M (1989) J Micr 159:143–160
39. Lenz F (1954) Z Naturforsch. A9:185–204
40. Du Chesne A, Wenke K, Lieser G, Wenz G, Wegner G, in preparation
41. Cowie JMG (1982) In: Developements in Block Copolymers, Goodman I (ed) Appl Sci Publ, London, New York pp 1–35
42. Henkee CS, Thomas EL, Fetters LJ (1988) J Mat Sci 23:1685–1694
43. Anastasiadis SH, Russel TP, Satija SK, Majkrzak CF (1989) Phys Rev Lett 62:1852–1855
44. Green PF, Christensen TM, Russel TP, Jerome R (1990) J Chem Phys 92:1478–1482
45. Lieser G, unpublished results
46. Inoue T, Soen T, Hashimoto T, Kawai H (1969) J Polym Sci, Polymer Phys Ed A2 7:1283
47. Inoue T, Soen T, Hashimoto T, Kawai H (1970) In: Block copolymers, Aggarwal SL (ed) Plenum Press, New York, London, pp 53
48. Thomas EL, Alward DB, Kinning DJ, Martin DC, Handlin DL Jr, Fetters LJ (1986) Macromolecules 19:2197–2202
49. Hasegawa H, Tanaka H, Yamasaki K, Hashimoto T (1987) Macromolecules 20:1651–1662
50. Reich S, Cohen Y (1981) J Polymer Sci, Polymer Phys Ed. 19:1255–1267
51. Bethe H (1930) Ann Physik, Vol 5, Leipzig, pp. 325–400

Received April 26, 1994;
accepted May 19, 1994

Authors' address:

Dr. G. Lieser
Max-Planck-Institut für Polymerforschung
Postfach 31 48
55021 Mainz, FRG